Eur Biophys J (2012) 41:461–474
DOI 10.1007/s00249-012-0800-1

ORIGINAL PAPER

EBSA
Biophysics in Europe

# The dynamics of melittin-induced membrane permeability

**Gašper Kokot · Mojca Mally · Saša Svetina**

Received: 8 August 2011 / Revised: 24 February 2012 / Accepted: 6 March 2012 / Published online: 24 March 2012


**Abstract** The transport of co-encapsulated solutes through the melittin-induced pores in the membrane of giant phospholipid vesicles was studied, and the characteristics of the pore formation process were modeled. Molecules of two different sizes (dextran and the smaller, fluorescent marker Alexa Fluor) were encapsulated inside the vesicles. The chosen individual vesicles were then transferred by micromanipulation from the stock suspension to the environment with the melittin (MLT). The vesicles were observed optically with a phase-contrast microscope and by monitoring the fluorescence signal. Such an experimental setup enabled an analysis of a single vesicle's response to the MLT on the basis of simultaneous, separate measurements of the outflow of both types of encapsulated molecules through the MLT-induced pores in the membrane. The mechanisms of the MLT's action were suggested in a model for MLT pore formation, with oligomeric pores continuously assembling and dissociating in the membrane. Based on the model, the results of the experiments were explained as a consequence of the membrane's permeability dynamics, with a continuously changing distribution of pores in the membrane with regard to their size and number. The relatively stable "average MLT pore" characteristics can be deduced from the proposed model.

**Keywords** Single GUV study · Pore formation mechanisms · Membrane permeability · Melittin partition

G. Kokot · S. Svetina
Jožef Stefan Institute, Ljubljana, Slovenia

M. Mally (✉) · S. Svetina
Faculty of Medicine, Institute of Biophysics,
University of Ljubljana, Lipičeva 2,
1000 Ljubljana, Slovenia
e-mail: mojca.mally@mf.uni-lj.si

## Introduction

Melittin (MLT), one of the main constituents of bee venom, is a thoroughly studied amphiphilic peptide, and its characteristics and interactions with model and cell membranes have been closely examined [reviewed in Raghuraman and Chattopadhyay (2007)]. The ability of MLT to permeabilize lipid membranes is influenced by the membrane lipid composition: due to the MLT molecule net charge of +5 to +6 $e_0$ the binding of the MLT to the negatively charged membranes is enhanced compared to the neutral membranes (Beschiaschvili and Seelig 1990; Torrens et al. 2007). When studying the capability of MLT to permeabilize the membranes, it has been found that the effects of MLT are concentration dependent: at low concentrations the morphological perturbations of the membrane can be observed as the MLT monomers bind to the outer membrane layer (Hristova et al. 2001; Mally et al. 2007). At higher concentrations the permeation of the membranes is ascribed to the association of MLT helices leading to the formation of oligomeric pores (Katsu et al. 1988; Ladokhin et al. 1997; Matsuzaki et al. 1997; Hristova et al. 2001; Lee et al. 2004; Mally et al. 2007). The reported pore sizes range from 1 to 6 nm (Raghuraman and Chattopadhyay 2007) depending on the different experimental conditions (pH, temperature, membrane lipid composition). It has been established that pores form only after a certain peptide-to-lipid threshold concentration in the vesicle membrane is reached (Lee et al. 2004; Huang et al. 2004). A larger peptide-to-lipid molar ratio in the membrane yields larger pores (Schwarz et al. 1992; Matsuzaki et al. 1997) with more MLT monomers in the pore rim. In the study of Huang et al. (2004), it was hypothesized that the induced pores are, under a given set of conditions, all of the same size, their formation

resembling a phase transition from the state of no pores to the state of multiple, identical pores. Other studies report on a rather wide distribution of MLT pore sizes in a membrane under given conditions [for example in Ladokhin et al. (1997)]. The average value of the pore diameter is estimated in such studies.

From the experiments investigating melittin-induced vesicle leakage, it was found that for bilayers with similar melittin-binding properties the leakage depends on their area compressibility modulus and spontaneous curvature, but is not dependent on the bilayer hydrocarbon thickness (Allende et al. 2005). The pores are therefore best described as toroidal openings in the membrane with the lipid molecules inserted in between the MLT molecules in the pore rim and tilted perpendicularly to the normal of the membrane (Yang et al. 2001; Allende et al. 2005; Mihajlovic and Lazaridis 2010). MLT molecules adopt an α-helix structure when they are in contact with a lipid environment and are pictured as slightly bent rods (Terwilliger and Eisenberg 1982), with polar and charged amino groups facing the aqueous moiety. The bent-rod form of an amphipathic MLT helix may explain the relative stability of the MLT pores as bent MLT molecules drift from a flat part of the membrane to a preferred position on the curved part of the pore and become a component of a pore rim (Mihajlovic and Lazaridis 2010). In a dynamic molecular simulation of a pore, initially consisting of four MLT monomers, it has been shown that lipid molecules intercalate between MLT monomers to enable an energetically favorable pore expansion, caused by the electrostatic repulsion among the MLT molecules (Lin and Baumgaertner 2000).

The described characteristics of the MLT are in accord with the fact that MLT has, at a high enough concentration, a lytic effect on cells [reviewed in Dempsey (1990)], but the dynamics of the permeabilization process, potentially leading to cell lysis, is not clear. It has been established that at a given MLT concentration after the formation process the pores are stable (Ladokhin et al. 1997; Yang et al. 2001; Naito et al. 2000; Chen et al. 2003; dos Santos Cabrera et al. 2004; Huang et al. 2004; Allende et al. 2005; Macháň et al. 2010); however, in our previous work with single giant vesicles, we investigated the interactions between the vesicles and MLT, and showed that in a wide range of MLT concentrations the MLT-induced membrane permeability is increasing with MLT concentration and also with time at a given concentration (Mally et al. 2007). Namely, the osmotically tensed vesicles underwent a series of bursts, with vesicle membrane resealing after each burst. Both the decreasing of time intervals between the bursts and the shape of the curve, describing the leakage of the solute molecules from the vesicles, supported the conclusion that MLT-induced membrane permeability is increasing with time throughout the experiment. Since porous-membrane permeability is proportional to pore size and pore number, this finding led to the hypothesis that MLT pores are increasing in size and/or number by integrating new MLT monomers from the surrounding solution into the existing pores or by re-formation of the existing pores with time. These experiments could not distinguish between the two possibilities that present themselves as the major cause for the membrane's permeability increasing. We therefore designed an experiment to establish whether, at a constant MLT concentration, the membrane permeability increases as a consequence of the increasing number of MLT pores in the membrane or of the increasing size of the pores with time.

In the present study of the permeabilization dynamics we focused on elucidating the mechanisms of the MLT permeabilization of giant unilamellar vesicle (GUV) membranes. Since lipid vesicles are, due to their simplicity, an excellent model system to study the interactions between the membranes and various substances, they have also been frequently used in the context of MLT permeabilization studies. We have applied the methodology developed previously (Mally et al. 2002) that allowed us to continuously optically monitor single-cell-size vesicles responding to various peptides and proteins. The hypothesis was that in the case that the MLT-induced pore radius is increasing during the experiment we would be able to observe a delay in the beginning of the outflow of molecules of different sizes. A study of POPC LUVs co-encapsulating fluorescently marked dextran molecules of two different sizes (FD-4 and FD-70 dextran) was conducted previously (Ladokhin et al. 1997) to estimate the size of the MLT-pores: using the column gel-filtration of loaded LUVs it has been shown that about 88 % of the smaller FD-4 leaked out of the vesicles, compared to a 22 % elution of the FD-70, and the MLT pore diameter was hence calculated to be 2.5–3 nm. The dynamics of pore formation and the time dependence of the membrane permeability were not addressed in this study.

We have devised the experiments in such a way as to enable the vesicle membranes to remain flaccid throughout the experiment in order to exclude the potential influence of an increased membrane tension on the membrane-permeability increase. We performed the experiments on spherical GUVs with an encapsulated mixture of glucose and dextran (D) solutions with the fluorescent marker Alexa Fluor (AF). The vesicles were initially dispersed in an isomolar glucose solution and then micromanipulated into the environment of an isomolar glucose solution with MLT at a chosen concentration. The technique of phase-contrast microscopy made it possible to monitor the dextran (large encapsulated molecules) concentration inside the vesicle, and by using the intensity of the fluorescent signal in a fluorescent microscopy image we were able to

estimate the concentration of AF (small encapsulated molecules) inside the vesicle, as described in the Results section. A comparison of the two sets of measurements was the basis for a model describing the pore formation dynamics and the MLT-induced transport through the pores. A possible mechanism for MLT pore growth is modeled in the Results section and evaluated in the Discussion section. The findings are then placed in the context of previous studies, discussing the possible transient nature of individual MLT-induced pores in the membrane and the relatively stable "average pore" characteristics.

## Materials and methods

### Materials

The vesicle membranes were made from phosphatidylcholine [1-palmitoyl-2-oleoyl-*sn*-glycero-3-phosphocholine (POPC) (Avanti Polar Lipids Inc., Alabaster, AL, USA)]. The lipid is available in powder form; it was dissolved in a mixture of 2:1 (v/v) chloroform–methanol to 1 mg/ml. The solution was stored at −15 °C. Anhydrous, pro analysis (p.a.) glucose with a molar weight $M_w = 180.16$ g/mol and dextran 6000 ($M_w = 6$ kg/mol, Fluka, Switzerland) were used without purification. The sugar solutions were buffered (pH 7.4) with Trizma buffer (Trizma base and Trizma hydrochloride), obtained from Sigma Chemical Co. (St. Louis, MO). Alexa Fluor 594 hydrazide, sodium salt was purchased as a fluorescent marker at Molecular Probes Inc (Eugene, OR). Its excitation wavelength is 588 nm, and the emission wavelength is 613 nm. The melittin (from bee venom) was from Calbiochem, Merck Bioscences, Darmstadt, Germany. The HPLC showed the purity of the sample to be 97 % (data from the producer). Based on our experience and as noted in Yang et al. (2001), no difference in effects on the lipid membranes can be found in this type of study between purified and synthetic MLT as long as there was no added $Ca^{2+}$, needed for phospholipase activity, in the sample. The toxin was dissolved in water at a concentration 1 mg/ml and stored at 4 °C.

### Preparation of the vesicles

The phospholipid vesicles were prepared by electro-formation using a slightly modified version of the method of Angelova et al. (1992). The procedure of vesicle preparation and the experimental equipment for the vesicle manipulation and observation are described in detail in Mally et al. (2002). The vesicles were made to encapsulate the 0.19 M glucose, the 0.01 M dextran 6000, the 3 μM fluorescent marker Alexa Fluor 594 and 3 mM Trizma buffer, and then suspended in an isomolar (0.2 M) glucose solution to obtain a sample of unilamellar spherical vesicles.

Since experience shows that the vesicles produced using this method can have tethers and other protuberances when fresh, we used at least 1-day-old vesicles in order to allow the membrane to achieve its relaxed state. The control experiments with epifluorescence microscopy (not shown) demonstrated that after 24 h the majority of the vesicles were without tethers and protuberances.

### Experimental setting

The vesicles were observed under an inverted optical microscope (Nikon Diaphot 200) with a phase-contrast plate and a prism for the fluorescence-microscopy technique. The phase-contrast microscopy technique makes transparent objects visible by exploiting the refraction properties of the observed object and of its surroundings. When observed in the environment of a glucose solution, vesicles with entrapped glucose, dextran and AF solutions appear dark against the background as the refraction index of the inner solution is higher than that of the outer (glucose) solution. A characteristic white halo appears around the vesicle (Fig. 1a) in a phase-contrast image. The brightness of the halo depends on the difference of the refraction indices of the object and the surroundings, the size of the observed object, and on the properties of the microscope (Pluta 1989). We used this otherwise unwelcome effect of phase-contrast microscopy to obtain information about the composition of the vesicles' inner solution (as demonstrated in Fig. 1a, b), (Mally et al. 2002). Briefly, by analyzing a number of vesicles with a known composition of the inner solution, we obtained a calibration curve that determines the relationship between the halo intensity and the dextran concentration (Fig. 2a). In fluorescent-microscopy images the peak brightness level corresponds to the AF fraction inside the vesicle (Fig. 1c, d), and calibration curves were established for determining both the AF concentration (Fig. 2b) and the AF bleaching properties (Fig. 2c).

### Experimental procedure

Vesicles from the sample were selected, one at a time, with the criteria being that they had no visible protuberances and were unilamellar. The chosen vesicle was fully aspirated into a micropipette filled with glucose solution, and transferred into the chamber that was filled with 0.2 M glucose solution containing MLT at a given concentration ($c_{MLT} = 2$ μM), chosen according to the MLT-concentration range (Mally et al. 2007), where the increasing of membrane permeability was evidenced. The volume of the

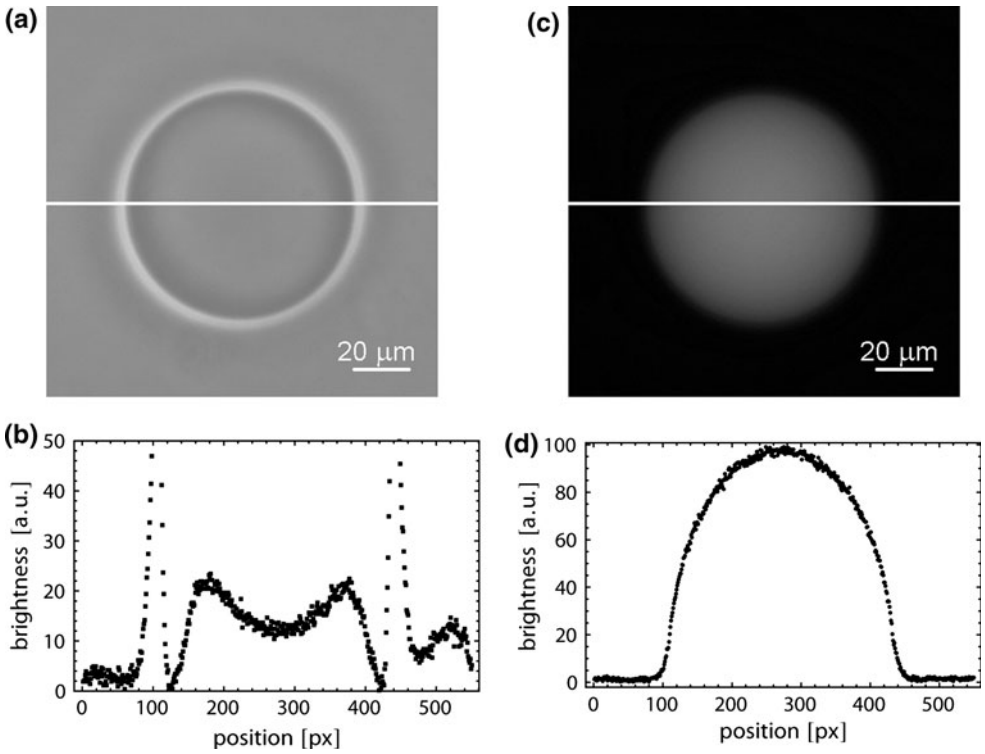


**Fig. 1** **a** A phase-contrast image of a typical vesicle used in the experiment and **b** a measurement of the brightness (in arbitrary units) of the vesicle cross-section along the indicated *line* to determine the peak-brightness level of the halo. **c** A fluorescence image of the same vesicle and **d** the measurement of the brightness (in arbitrary units) of the vesicle cross-section along the indicated *line* to determine the peak-brightness level of the vesicle cross-section

vesicle is negligibly small compared to the volume of the experimental chamber with the MLT solution, and therefore we can assume that the concentration of free MLT in the solution is constant and the concentrations of AF and dextran outside the vesicle are zero throughout the experiment. All the experiments were carried out at room temperature.

The vesicles were monitored and the experiments recorded as a series of digital images, which were saved for later analysis. The images were captured and the shutter of the UV lamp was controlled using adapted Wasabi software. The light for the phase-contrast microscopy during the measurement of the fluorescence signal was obstructed manually. The time interval between capturing the phase-contrast image and the fluorescence image was 1.5 s, which was the shortest achievable time interval needed to optimize the focusing of the vesicle before each image was captured. ImageJ software (Rasband 1997–2012) was used for the image processing. The background was removed by the rolling-ball algorithm that is already implemented in the software. From each image we determined the radius of the vesicle ($R$) and the brightness level either of the vesicle halo in the phase-contrast images or the brightness level of the fluorescence signal from the AF in the fluorescence images. From the vesicle phase-contrast microscopy image analysis the time dependence of the halo brightness level was measured. The decrease of the halo brightness level with time was correlated with the decrease of the dextran fraction (and the increase of the glucose fraction) in the vesicle inner solution. The vesicle-fluorescence image analysis gave us the dependence of the peak-brightness level with time. After adjusting for bleaching, the measurements were correlated to the decrease of the AF concentration in the vesicle inner solution with time.

The decrease of the solute concentration depends on the membrane permeability ($P_{\mathrm{AF,D}}$), a proportionality factor between the molar concentration of the solute inside the vesicle ($c_{\mathrm{AF,\ D}}$) and the induced solute outflow ($J$, $J_{\mathrm{AF,\ D}} = \mathrm{d}(c_{\mathrm{AF,D}}V)/\mathrm{d}t$):

$$J_{\mathrm{AF,D}} = -P_{\mathrm{AF,D}} A c_{\mathrm{AF,D}}, \tag{1}$$

where the indices AF and D stand for the Alexa Fluor and the dextran, respectively, and $A$ is the surface area of the vesicle membrane. Considering the constant vesicle volume ($V$), linearity between the light intensity ($I$), read as the brightness level in the densiometric plots, and the concentration of the solvent inside the vesicle (Fig. 2), integration over $c$ yields:

$$\left(\ln\frac{I}{I_0}\right)_{\mathrm{AF,D}} = -\frac{3}{R}\int_0^t P_{\mathrm{AF,D}}\mathrm{d}t, \tag{2}$$

with the implicit assumption that the membrane permeability is not constant, but exhibits a dependence on time that follows the pore formation dynamics. For a given vesicle the analysis of the measured brightness levels with respect to time gives us information about the dynamics of the membrane permeability.

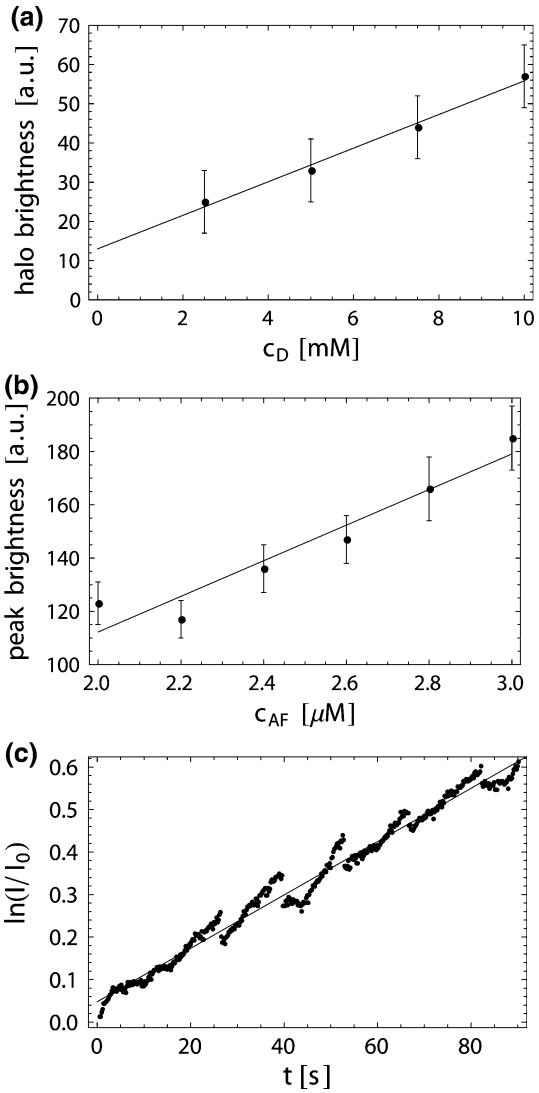


**Fig. 2** Calibration curves determining the dependence of the brightness level in the vesicle image on the solute concentration. **a** The dependence of the peak-brightness level of the vesicle halo on the dextran concentration. **b** The dependence of the peak-brightness level of the vesicle cross-section on the AF concentration. **c** Exponential dependence of the AF signal on the illumination time of the vesicle was investigated. A bleaching parameter (*slope of the curve*) was determined by successive fluorescence imaging of one vesicle and observing the logarithm of intensity normalized by its initial value versus the time of illumination. The jumps correspond to the focusing optimization of the observed vesicle during the measurement

## Results

### Observations

For the concentrations of MLT used in this study the observed vesicles were at all times spherical, and remained flaccid. The experiments were analyzed in order to obtain the records of the changing of the vesicle contents (AF and

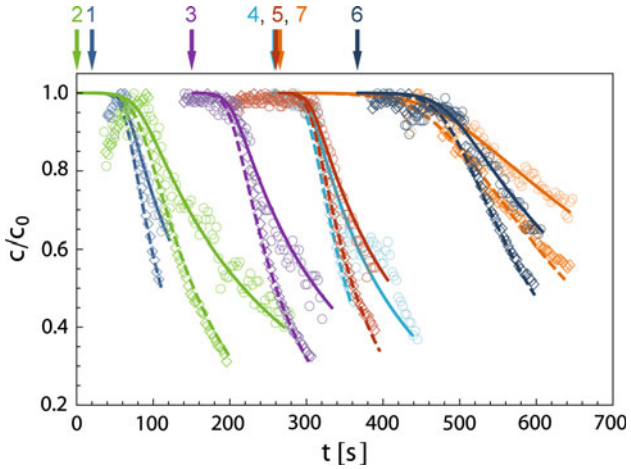


**Fig. 3** Dependence of the normalized inner solution concentrations on time for seven of the analyzed vesicles. The measured outflow data set for dextran is represented by *circles* and for AF by *diamonds*. Time $t = 0$ denotes a transfer of the vesicle into the MLT solution. Model predictions (Eqs. 2–7) with fitted model parameters for respective solution concentrations are shown as *full lines* for the dextran and *dashed lines* for Alexa Fluor concentrations with respect to time. The *arrows* point out the time $t'$ at which the modeled pore formation process begins. The model parameters used for the model-prediction computations are the same for all the analyzed vesicles, except for the $k_{on,0}$ parameter and the vesicle radius (in the interval between 36 and 42 μm for the vesicles shown), which are adjusted for each vesicle individually

D concentrations) over time as described in the previous section. After the initial plateau (Fig. 3), where the vesicle brightness levels are constant (and we can conclude that the membrane is either not yet permeabilized or that the pores are not large enough to enable the passage of the solute molecules), it is evident that the halo brightness is diminishing with time in the phase-contrast image, and that the contrast between the gray levels inside and outside the vesicle is diminishing in the fluorescence image, meaning that the concentrations of both the dextran and the AF inside the vesicle are diminishing. The time lag (the plateau illustrating the time interval before the observable leakage) is different for each vesicle (from around 30 s to as much as 8 min, see Fig. 3). In the control experiments where the vesicles were transferred to glucose solution without MLT the vesicles remained the same with respect to their shape and the brightness signal for long periods (>1 h). However, also in the presence of MLT a significant fraction of vesicles is not permeabilized by any observable criterion—they also maintain their shape and brightness signal for long periods (>20 min).

For the majority of vesicles the results of the experiment imply the permeabilization of the vesicle membrane by MLT and the transport of the dextran and AF molecules from the vesicle to the outer solution. The leakage curve, describing the diminishing of the solute concentration

inside the vesicle, exhibits a relatively sharp break after the initial lag-time plateau and becomes less steep after the concentration of the solute falls below approximately 50 % of the initial value. The leakage of two types of solute molecules from the individual vesicle is described by two distinct measurement data sets. The diminishing of the AF concentration with respect to time is clearly faster compared to the dextran leakage from the analyzed vesicle, yet there is no observable delay between the onset of the leakage of the smaller AF and larger dextran molecules from the vesicle. The obtained results suggest some qualitative conclusions about the behavior of the treated system: first, that the outflow is size—regulated, yielding two separate curves describing two different solutes' concentrations with respect to time; second, that the formed pores have a rather wide size distribution (there is no delay between the noticeable outflow of the smaller and the larger molecules); third, that membrane permeability increases at first (the leakage curve is steep after the plateau) and becomes more or less constant afterwards (the leakage curve becomes pronouncedly less steep for both types of solutes), implying reorganization or re-formation of MLT pores; and fourth, that membrane permeabilization is initiated stochastically (the time-lags are different for different vesicles in the same experimental conditions).

Our intention was to describe the observed vesicle behavior with a plausible physical mechanism. A possible model for the pore formation mechanisms, consistent with the measurements on membrane permeabilization, is presented in the next section.

## Model

A simple model with assumed constant membrane permeability does not describe the measurements, whereas phenomenological model descriptions of membrane permeability as first increasing and then with a stabilized value can describe the efflux curves, but not the time lag, and they also do not give an insight into the underlying mechanisms for such a membrane permeability dynamics (increasing at first and constant later on). In order to frame the observations within a consistent model we first state the assumptions regarding the observed processes: (1) MLT molecules partition from the bulk solution to the vesicle membranes, having a parallel orientation with the membrane surface plane while bound to the membrane as monomers; (2) MLT monomer adopts a trans-bilayer, i.e., orthogonal to the membrane surface-plane orientation when in an interaction with at least one other MLT monomer; (3) MLT molecules are positively charged and bound MLT increases the surface electric potential of the membrane, consequently diminishing the MLT partition coefficient; and (4) the volume of the vesicle is constant throughout the experiment.

It is attempted to model a scenario of pore formation that supports all the observed phenomena while taking into account the established properties of MLT from previous studies. In particular a theoretical study by Zemel et al. (2003) presents itself as an appropriate reference when considering toroidal membrane pores with charged constituents, although their approach will be simplified for the needs of the description of our model situation. We considered that MLT forms multimeric trans-bilayer pores with a pore rim comprising both MLT and lipid molecules and that at a neutral pH the MLT molecule has a positive net-charge ($e = Ze_0$, with $Z = +5$). We modeled a pore with at least three MLT monomers ($n \geq 3$) as an opening with radius $R_{\mathrm{p},n}$ with $n$ point charges evenly positioned along the pore circumference. The energy of such a pore involves the line tension, electrostatic interactions between MLT charges, and a term describing the released energy for each MLT monomer attaining a trans-bilayer position as a part of a pore rim: The corresponding sum can be written for odd and even values of the number of MLT monomers in the pore, respectively, as

$$E_{n,\mathrm{odd}} = 2\pi R_{\mathrm{p},n}\Gamma + \frac{n(Ze_0)^2}{8\pi\varepsilon\varepsilon_0 R_{\mathrm{p},n}} \sum_{k=1}^{\frac{n-1}{2}} \frac{1}{\sin\frac{k\pi}{n}} - n\delta, \tag{3a}$$

$$E_{n,\mathrm{even}} = 2\pi R_{\mathrm{p},n}\Gamma + \frac{n(Ze_0)^2}{8\pi\varepsilon\varepsilon_0 R_{\mathrm{p},n}} \sum_{k=1}^{\frac{n}{2}} \left( \frac{1}{\sin\frac{k\pi}{n}} - \frac{1}{2} \right) - n\delta, \tag{3b}$$

with $\Gamma$ being the line tension for a pore in a POPC membrane, $\varepsilon$ the dielectric constant for water and $\delta$ the energy difference between two positions of a MLT monomer—before and after joining into the pore rim. Thus, a discrete energy level value is ascribed to each $n$-meric pore. By minimizing the energy of a pore (Eqs. 3a, 3b) with respect to the pore radius $R_{\mathrm{p},n}$ we can find the optimal pore size for a given number of MLT monomers in the pore:

$$R_{n,\mathrm{odd}} = \frac{Ze_0}{4\pi} \left( \frac{n}{\Gamma\varepsilon\varepsilon_0} \sum_{k=1}^{\frac{n-1}{2}} \frac{1}{\sin\frac{k\pi}{n}} \right)^{\frac{1}{2}}, \tag{4a}$$

$$R_{n,\mathrm{even}} = \frac{Ze_0}{4\pi} \left( \frac{n}{\Gamma\varepsilon\varepsilon_0} \left( \sum_{k=1}^{\frac{n}{2}} \frac{1}{\sin\frac{k\pi}{n}} - \frac{1}{2} \right) \right)^{\frac{1}{2}}. \tag{4b}$$

By inserting the obtained radii into Eqs. (3a), (3b), the energy levels of the pores with discrete radii can be determined with respect to the number of MLT monomers in the pore (Fig. 4). The choice of the interrelated parameters' values [i.e., $\delta$ and the product of $Z/(\Gamma\varepsilon)$] determines the number of the MLT monomers that correspond to the energetically minimal MLT pore.

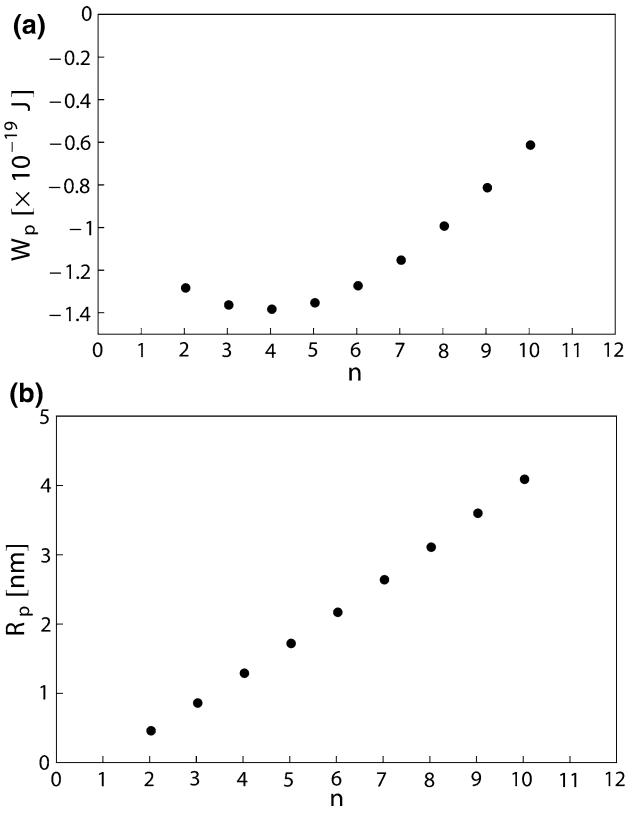


**Fig. 4** Characteristics of melittin pore as predicted by Eqs. 3a, 3b and 4a, 4b. The sum of the relevant energy contributions ($W_p$) for the MLT pore (**a**) and the radius of the pore with respect to the number of MLT monomers ($n$) in the pore rim (**b**)

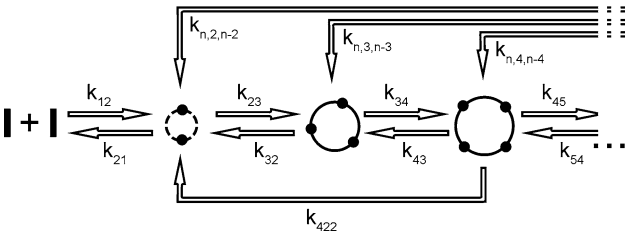


**Fig. 5** A schematic representation of the MLT pore formation kinetics. MLT monomers are denoted as *black rectangles* when lying parallel to the membrane and as *black circles* when in a trans-bilayer position, forming a pore rim (the rim marked with a *circle*)

In our previous work (Mally et al. 2007) we showed that at low MLT concentrations binding of MLT to the outer membrane causes the leaflet-area difference first to increase and then to decrease with time with a square dependence on MLT concentration, stressing the role of MLT pairs as vehicles for both MLT and lipid molecules' translocation. In a proposed kinetic model for the assembly and disassembly of multimeric structures (schematically shown in Fig. 5), the first step of the pore formation process is thus two MLT monomers joining into a short-lived dimeric pre-pore. The pores can grow by another monomer becoming a part of a pore rim and dissociate by a monomer separating from the pore rim. At any given moment the proposed model assumes the coexistence of different MLT structures [monomers, dimers and $n$-meric ($n \geq 3$) MLT pores] in the membrane. The number concentration of respective structures in the membrane is defined as $c_n = N_{p,n}/N_L$ (with $N_{p,n}$ being the number of $n$-meric structures and $N_L$ being the number of lipid molecules in the membrane) and the time dependence of the respective pore concentrations can be deduced from a set of kinetic equations, described in the following section.

The equation for the time dependence of the number concentration of monomers ($c_1$) and of the dimers and pores ($c_n$) in the membrane must be written separately. For monomers we have:

$$\frac{dc_1}{dt} = k_{on}c_0 - k_{off}c_1 - 2k_{1,2}c_1^2 + \sum_{n=2}^{n_{max}} \left(k_{n,n-1,1}c_n - k_{n-1,n}c_1c_n\right), \quad (5)$$

where the coefficients $k_{on}$ and $k_{off}$ are the MLT association and dissociation coefficients, respectively, for MLT molecules partitioning into the membrane from a bulk solution with the MLT concentration $c_0$. Upon binding to the membrane, positively charged MLT monomers increase the membrane surface potential and consequently reduce the partitioning of new MLT monomers from the bulk solution into the membrane; the association coefficient ($k_{on}$) is thus modeled as $k_{on} = k_{on,0}e^{-Ze_0\Phi_0(t)/kT}$ [from Schwarz (1996)], where $\Phi_0$ is the membrane surface potential, changing concomitantly with the number of MLT molecules in the membrane over time. Following the Gouy-Chapman approach the membrane potential can be determined from the relation $\Phi_0(t) = 2kT/e_0(Arcsinh(\sigma(t)/(8\ I\ \varepsilon\varepsilon_0\ kT)^{1/2}))$, where $\sigma$ is the surface-charge density of the membrane [calculated from $\sigma(t) = Z_{eff}\ e_0\ N_{MLT}(t)/(N_L a_L)$, with $Z_{eff}e_0$ as an estimate of the effective charge of a MLT monomer in the POPC membrane, $N_{MLT}(t)$ the sum of all the MLT molecules in the membrane and $a_L$ the surface area of one lipid molecule] and $I$ is the ionic strength. In the assumed scenario the bound MLT monomers continuously traverse from the plane of the membrane into the orthogonal position when they pair with another MLT monomer or when they become a part of an existing—pore rim, and can be released from the pore rim back to the monomeric state parallelly in the membrane. The kinetic parameters of the form $k_{n-1,n}$ are the association kinetic parameters with $n-1$ denoting the initial number and $n$ the final number of monomers in the pore rim. For the dissociation coefficients $k_{n,n-1,1}$ we take into consideration the energy difference $\Delta E_{n,n-1} = E_n - E_{n-1}$ between the energies of the $n$-meric and the $n-1$-meric

pores so that the dissociation coefficients are of the form $k_{n,n-1,1} = k_{d0,1}\, n\, e^{-\Delta E_{n,n-1}/kT}$. A pore with $n$ monomers has $n$ possibilities for a monomer dissociation, and thus the dissociation coefficients are taken to be proportional to the number of monomers in the pore. The probability of a monomer encountering an existing pore and joining the pore rim has to be proportional to the dimension of the pore, and therefore the association coefficient is taken to be proportional to the pore circumference and in that way proportional to the number of monomers already contained in the pore rim that the monomer is about to join, $k_{n,n+1} = k_{a0}n$. The model thus accommodates the assumption that all the kinetic parameters are (linearly) proportional to the pore size, while the parameters $k_{d0}$ and $k_{a0}$ are taken to be size independent.

The pore formation process can be expressed by a set of differential equations describing the time dependence of the concentration of pores with $n$ melittins ($c_n$, $n \geq 2$). The equations for pore formation kinetics can be given in a general form as:

$$\frac{\mathrm{d}c_n}{\mathrm{d}t} = k_{n-1,n}c_1c_{n-1} - k_{n,n+1}c_1c_n + \sum_{i=1}^{n_{\max}-n} k_{n+i,n,i}c_{n+i} - \sum_{i=1}^{\left[\frac{n}{2}\right]} pk_{n,n-i,i}c_n, \quad (6)$$

where the first and the second term describe the association of monomers to existing pores in the membrane (as described in the Eq. 5). A pore can thus form by a MLT monomer sliding into an existing pre-pore (dimer) and grow by another MLT monomer joining the existing pore rim. The pores can dissociate by a monomer separating from the pore rim and also by fission of a large pore into two smaller pores (the third and the fourth term in Eq. 6). The parameters of the form $k_{n,n-i,i}$ are the dissociation kinetic parameters with $n - i$ and $i$ denoting the final numbers of monomers in the pore rims of two new pores, formed from the initial pore with $n$ monomers. Analogously to the formalism for determining the dissociation coefficients $k_{n,n-1,1}$ (Eq. 5), for the dissociation coefficients $k_{n,n-i,i}$, we take into consideration the energy difference $\Delta E_{n,n-i,i} = E_n - (E_{n-i} + E_i)$ between the energy of a $n$-meric pore and the sum of the energies of the $i$- and $n - i$-meric pores so that the dissociation coefficients are of the form $k_{n,n-i,i} = k_{d0}\, n\, e^{-\Delta E_{n,n-i,i}/kT}$. A pore with $n$ monomers has $n$ possibilities for dissociation into two new formations with $n - i$ and $i$ monomers (with the assumption that the monomers are not permutated along the pore rim) and thus both the dissociation and association coefficients are again proportional to the number of monomers in the pore. The parameter $p$ has the value of ½ in the special case when $i = n/2$ and the number of possibilities for pore dissociation is halved, and equals $p = 1$ in all other cases.

By solving the set of differential equations (Eqs. 5 and 6) with the free parameters $k_{d0}$ (with a different parameter value for a monomer dissociating from a pore, $k_{d0,1}$) and $k_{a0}$ we can model the dependence of the monomer and $n$-meric pore concentrations in the membrane on time. The maximum number of monomers that is accounted for in the calculations is set to ten monomers in the pore rim ($n_{\max} = 10$). The results of the calculation are illustrated in Fig. 6, with the kinetic parameter values chosen to qualitatively describe the results presented in Fig. 3. The model scenario thus assumes that the concentration of monomers in the membrane at $t = 0$ is zero and increases rapidly to a maximum value, enabling the formation of dimers and pores (Fig. 6a, b). Monomers are continuously incorporating into the membrane, increasing the numbers of pores in the membrane throughout the process. The changing of the number of bound melittins in the membrane (Fig. 6c) affects the membrane surface potential and influences the partitioning of new MLT molecules from the bulk solution into the membrane (Fig. 6d). The fraction of MLT monomers in the membrane decreases as the MLT molecules become involved in the pore rims (Fig. 6e). The individual pores are continuously reforming, and the distribution of pore sizes changes with time, narrowing towards a peak at a pore with 4 MLT molecules in the pore rim (Fig. 6f).

We have modeled the time dependence of the membrane permeability on the basis of the distribution of the number of pores with respect to their sizes over time. For the permeability of the membrane with MLT-induced pores we use the expression:

$$P_{\mathrm{AF,D}} = \sum_{n=n_{\mathrm{AF}},n_{\mathrm{D}}}^{n_{\max}} c_n \alpha_{\mathrm{AF,D}} \pi \left(R_{\mathrm{p},n} - r_{\mathrm{AF,D}}\right)^2 \quad (7)$$

where $\alpha_{\mathrm{AF,\,D}}$ is a proportionality parameter and $r_{\mathrm{AF,\,D}}$ is the size measure of the Alexa Fluor and dextran solute molecule, respectively. The membrane permeability is therefore the sum of the permeabilities of all the pores in the membrane that are large enough to enable the passage of a solute molecule. The phenomenological description of induced permeability is based on the assumption that MLT pores can be modeled as two-dimensional openings in the membrane with the length of the MLT pores in the POPC membranes comparable to the size of the solute molecules. The parameter $\alpha_{\mathrm{AF,D}}$ can be interpreted as the probability for the molecules of a certain type to encounter a pore.

By investigating the number of MLT molecules in the membrane, the number of formed pores and the radii of the pores in the membrane through time (Fig. 6) and determining the sum of all the relevant pores that allow for the passage of the respective molecules (of the Alexa Fluor and of the larger dextran molecules), we can calculate the dependence of the membrane permeability on time

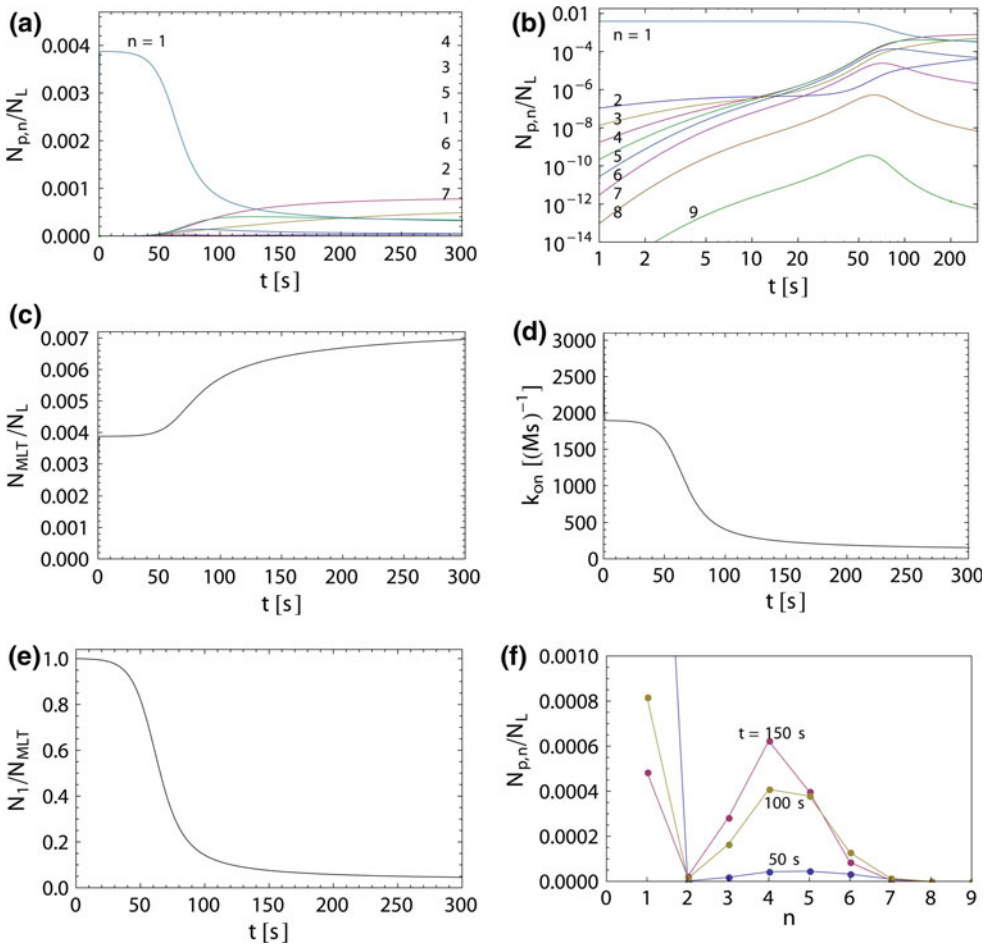


**Fig. 6** Illustrations of the modeled MLT pore formation kinetics. **a** Dependence of MLT monomer concentration in the membrane on time (*blue line*) compared to the time dependence of the concentrations of dimers, trimers, etc. (shown as $N_{p,n}/N_L$, where $N_{p,n}$ is a number of pores with $n$ monomers and $N_L$ is the number of lipid molecules) in the membrane. The legend on the *right* denotes the number of monomers ($n$) in the pore and refers to the *right-end* of the curves in the *graph*, from *top* to *bottom*. The pore concentrations at bulk concentration $c_0 = 2$ μM were determined on the basis of the model (Eqs. 2–7). A vesicle with radius $R = 40$ μm was modeled in this example. **b** Representation of the pore number concentration dynamics on a log–log scale. **c** Number concentration of MLT molecules ($N_{MLT}/N_L$, where $N_{MLT}$ is the number of all MLT molecules in the membrane) in the membrane with respect to time. **d** The diminishing of the $k_{on}$ parameter, describing the binding of the MLT monomers from the bulk solution to the membrane with respect to time. **e** The fraction of monomers ($N_1/N_{MLT}$) in the membrane with respect to time. **f** Distribution of MLT pores (shown as a number concentration of pores, $N_{p,n}/N_L$) in the vesicle membrane at three different times (after 50, 100 and 150 s), peaking at pores with 4 MLT monomers in the rim

(Fig. 7a) and obtain a prediction on the solute concentration with respect to time for different sizes of solute molecules (Fig. 7b). The probability for an AF molecule to encounter a pore is taken to be equal to that for a dextran molecule ($\alpha_{AF} = \alpha_D$).

The model predictions can now be compared to the measurements' data on the encapsulated solute concentrations with respect to time, as presented in Fig. 3. The model describes the concentration dynamics for both solutes inside the vesicles from $t = 0$ (the transfer of the vesicle into the solution with the MLT), with applying, for example, $k_{on,0} = 3.3 \times 10^4$/Ms for the second vesicle on the left-hand side in Fig. 3. Due to the slowly increasing number of relevant pores that enable the transport of solutes from the vesicle, the characteristic plateau illustrating the time interval before the observable leakage is inherent to the model. For other vesicles the measurement data could only be described by assuming a time lag ($t'$) before the initiation of the pore formation process described by the model. The values of the monomer and dimer concentrations at the end of the time-interval $t'$ were determined and taken into account as the initial conditions of the modeled pore formation process. Subsequently, the same model parameters ($k_{off}$, $k_{d0}$, $k_{d0,1}$, $k_{a0}$, $\alpha$) were applied for all the analyzed vesicles (except for the vesicle radius $R$, which was measured and accounted for in the model for each

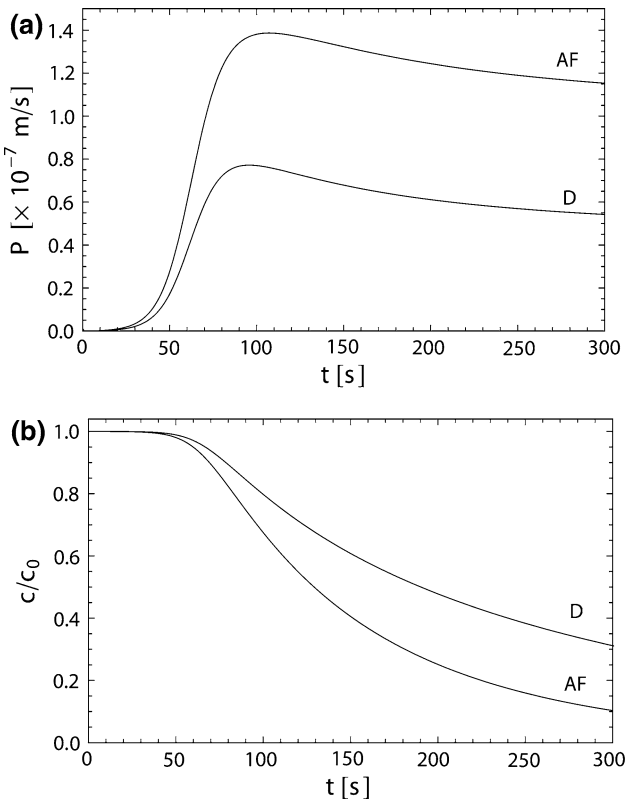


**Fig. 7** Model prediction of the membrane permeability. **a** Time dependence of MLT-induced membrane permeability ($P$) for two different types of encapsulated molecules [Alexa Fluor (AF) and dextran (D)] and **b** the resulting time course of normalized concentrations for D and AF

vesicle individually, and a variable $k_{on,0}$ parameter, describing the partition of the MLT monomers from the bulk solution into the membrane). With the free parameters of the model adjusted, a model gives a description of the observed concentration dynamics (Fig. 3, full and dashed lines, with arrows pointing out the beginning of the modeled pore formation process at $t'$).

## Discussion

In the experiments single GUVs with co-encapsulated solutions of Alexa Fluor and dextran were transferred into the solution with MLT, and we were able to observe different aspects of the MLT-induced membrane permeabilization (i.e., lag-time before the observable leakage, the shape of the leakage curve with a characteristic break at the end of the lag-time and the diminishing steepness of the curve, two different leakage curves for two different types of solute molecules). From the simultaneous measurements of the two solutions' concentrations, we obtained the information on the dynamics of the process, and we sought a consistent theoretical support for these experimental results. A model that we propose is a minimal theoretical framework to account for all the observed phenomena. In short, our model assumes the formation of pores of different sizes and different relative energies for which it was taken that electrostatic repulsion between the MLT molecules, the line tension of the induced pore rim, and the energy difference between the MLT molecule position outside and inside the pore rim are governing the behavior of the MLT molecules' ensemble in the membrane. The transition of single MLT molecules into and out of the pores and the fission of large pores (Fig. 5) lead to characteristic pore formation dynamics (Fig. 6b). The number concentrations of differently sized MLT pores are continuously changing, leading to an increasing number of pores that are permeable to dextran and Alexa Fluor molecules (Fig. 8a). The energetically favorable transformations of pores yield a changing distribution of pore sizes with a peak at an energetically favorable number of MLT monomers in the pore rim (Fig. 6f) and with a relatively stable average pore size (Fig. 8b). The resulting membrane permeability for dextran and Alexa Fluor at first increases and is later on stabilized (Fig. 7a).

The parameters of the suggested model can be subdivided into four groups: in the first group the parameters connected to the partitioning of the MLT molecules from the bulk solution into the membrane are assembled. The parameters of the second group describe the size of the pore, the third group are the kinetic parameters, and in the fourth group we collect the phenomenological parameters of the model. In general, the parameters were determined in a retrospective manner: the average pore size of around 1 nm suggests low numbers of MLT monomers in the pore rim, and we have set this energetically favorable monomer number to be $n_{MLT} = 4$ (Zemel et al. 2003); other free parameters' values (Eqs. 3a, 3b–7) are based on that choice.

First group parameters: The modeled partition of the MLT molecules from the bulk solution is continuous, with the partition coefficient modeled as $k_{on}(t) = k_{on,0}e^{-Ze_0\Phi_0(t)/kT}$, describing a diminishing MLT insertion into the membrane with respect to time (Fig. 6a) as a consequence of the increased membrane surface potential due to the positive charge of the bound MLT molecules. The surface-charge density of the membrane ($\sigma$) is linearly proportional to the number of MLT molecules in the membrane, with the proportionality factor formulated as $Z_{eff}e_0/(N_L a_L)$ and taking $Z_{eff}$ $e_0 = 2.5\ e_0$ as an estimate of the effective charge of a MLT monomer in the POPC membrane (with MLT monomers oriented perpendicularly in the membrane when included in the pore rim, only approximately half of the MLT charge is effectively contributing to the surface potential of each of the membrane leaflets). The number of lipid molecules in one membrane leaflet ($N_L$) is calculated from the vesicle's surface

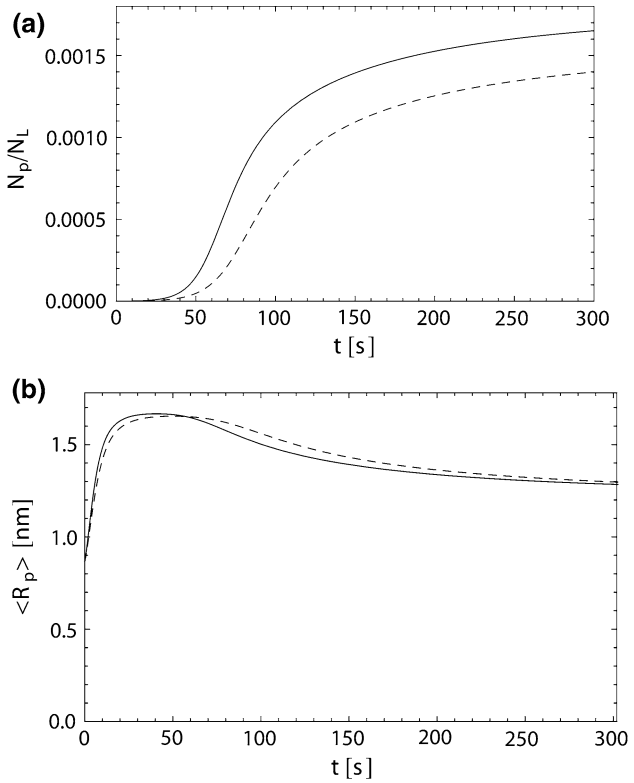


**Fig. 8** Average properties of MLT pores (with $n \geq 3$) in the membrane. Number concentration ($N_p/N_L$) of the sum of all MLT pores in the membrane with respect to time (**a**) and average MLT pore size with respect to time (**b**) at two MLT concentrations: $c_{MLT} = 2$ μM (*full*) and $c_{MLT} = 1$ μM (*dashed curves*)

area (with the radii of the analyzed vesicles from 36 to 42 μm) taking $a_L$ as the surface area of one POPC molecule ($a_L = 68$ Å$^2$). Rapid binding of the MLT to the vesicle membrane [in the order of milliseconds (Schwarz and Beschiaschvili 1989)] causes the initial value of the association coefficient $k_{on,0}$ to drop rapidly (within the first second), yielding an effective initial partition coefficient $K_{p,eff} = k_{on,0}/k_{off} \approx 2 \times 10^3$ M$^{-1}$ (Fig. 6d), in agreement with the reports on the MLT partition to POPC membranes (Kuchinka and Seelig 1989). The results of the present study imply an interval of values for the effective MLT partition coefficient ($K_{p,eff} = 10^3$–$2.5 \times 10^3$ M$^{-1}$) even though the experimental conditions are the same for all the observed vesicles. The reports about the measured $K_p$ for MLT that can be found in the literature vary by two orders of magnitude, from $K_p = 10^3$–$10^5$ M$^{-1}$ (Raghuraman and Chattopadhyay 2007).

The parameters of the second group: The size of the pore can be roughly described as proportional to the square root of the number of MLT monomers in the pore rim, with the proportionality ratio $Ze_0/(4\pi(\Gamma\varepsilon\varepsilon_0)^{1/2})$ governing the slope of the curve (Fig. 4b) and the dependence of the energy minimum on the number of MLT monomers in the pore. By adjusting the value of this ratio we place a desired number $n = 4$ as an optimal number of MLT monomers in the pore to correspond to the energy minimum of the pore. This yields pores with sizes that are in agreement with reports in the literature and makes the growth of pores toward large numbers of pore-constituting monomers less energetically favorable. The resulting estimate of a line tension ($\Gamma = 2.6 \times 10^{-11}$ N) is within the reported values interval for $\Gamma$ for PC membranes (Karatekin et al. 2003). The energy difference between two different MLT monomer positions in the membrane ($\delta$) is determined by analogous consideration ($\delta = 1.4 \times 10^{-19}$ J). The chosen value for $\delta$ is of the same order of magnitude as the estimate of the total interaction-energy difference between melittin in a lipid environment and melittin in water $\Delta E_{tot} = 2.3 \times 10^{-19}$ J (Manna and Mukhopadhyay 2009). The value for ionic strength ($I$) is 0.003 M in our experimental setting, and the dielectric constant for water ($\varepsilon$) is taken to equal 81. We did not distinguish between different dielectric constants for water inside the pore and in the outer solution as this does not contribute to the quality or clarity of the presented model.

The parameters of the third group are the kinetic coefficients describing the dynamics of the pore formation process (Eqs. 5 and 6) and were either taken from the references or determined as described in the Results section. The kinetic parameter values can be listed as follows: $k_{on,0} = 6 \times 10^4$/Ms, $k_{off} = 1$/s, [referring to the partition coefficient $K_{p,0} = k_{on,0}/k_{off} = 6 \times 10^4$/M from the study by Schwarz et al. (1992)]; dimer association and dissociation coefficients, $k_{1,2} = 0.01$/s and $k_{2,1} = 0.02$/s, (Schwarz et al. 1992), $k_{d0} = 10^{-18}$/s, $k_{d0,1} = 0.01$/s, $k_{a0} = 42$/s.

The fourth group comprises the parameters, assembled in the phenomenological equation for membrane permeability (Eq. 7). We have examined POPC membrane permeability with two different probes: the size of Alexa Fluor is estimated from the Stokes radius ([$r_{AF} = 0.74$ nm from Heyman and Burt (2008)]. On the other hand, the dextran molecule is asymmetrical, and, with dextran being a flexible polymer, it is better described as a random coil than a solid sphere (Venturoli and Rippe 2005), as suggested from the comparison of the measured values of the diffusion coefficient to the values, calculated on the basis of the Stokes radius [about 2.2 nm for dextran 6,000 (Hamm et al. 1999)]. Consistently the measured membrane permeabilities for dextran are higher than estimated from theoretical predictions (Venturoli and Rippe 2005). In our model we estimated an effective dextran molecule size to be 1 nm, which corresponds to the shorter axis of a solid ellipsoid estimate [with ellipsoid axis ratio 1:4 (Bohrer et al. 1979)] and fits the measured data for dextran permeability. With these values for solute molecules' sizes the proportionality parameter $\alpha_{AF,D}$, describing the "probability" of the solute

molecules to encounter a pore and pass through to the outer solution, was set to be the same for both types of molecules $\alpha = 5.4 \times 10^{13}$/(ms); implicit is an assumption that the diffusion effects do not play a significant role in the observed process of transport through the membrane and that therefore passing through a pore is regulated solely by the ratio of molecule-to-pore sizes.

The analysis of the system behavior suggests a continuous pore formation, yet three qualitatively different phases of the process can be deduced (see Fig. 6b with a log–log scale applied for a clearer representation): during the first phase the number of pores is increasing, but since the total number of MLT pores in the membrane is still very small, the membrane permeability for the encapsulated solutes is effectively zero, resulting in a characteristic time lag before the observable solute leakage. After the number of MLT pores reaches a certain value, in the second phase the number of pores begins to increase in a cooperative manner, which is a consequence of the proportionality of association and dissociation coefficients to $n$ (the number of monomers in the pore). With an increasing number of large pores ($n \geq 3$), there are, due to their fission, more and more dimers, which serve as pore precursors and are essential for the formation of new pores. During this phase the concentration of dimers grows to a new stationary level, and the membrane permeability for the encapsulated solute molecules exhibits a significant increase. The third phase is marked by a decrease of the monomer concentration in the membrane because of the concomitant increase of the membrane surface potential. The concentration of monomers falls to the level at which the production of multimeric MLT pores is sufficiently diminished. Numbers of MLT pores of different sizes slowly approach an equilibrium distribution, stabilizing the membrane permeability. Based on the results of this study we can conclude that the simultaneous onset of leakage corresponds to the simultaneous increasing of the membrane permeability for both types of solute molecules. Membrane-permeability dynamics is characterized by cooperative pore formation and by the conditions of passing through the formed pores (Eq. 7). We assumed that the probability of a solute molecule to encounter and pass through a pore is the same for both types of molecules, but the same results on the membrane permeability (Fig. 7) could have been obtained if the same size ($r_{AF,D}$), but different diffusion properties (and therefore different $\alpha_{AF}$ and $\alpha_D$) of the solute molecules are assumed. The most realistic description of the pore permeability in these experimental conditions is probably a combination of these two possibilities. It should therefore be stressed that it is not appropriate to emphasize the absolute values of the parameters of the suggested pore formation scenario, but it should be useful to evaluate the results with comparing them to the relevant studies on MLT-membrane interaction.

Our experiments were restricted to a single concentration of MLT in the bulk solution ($c_0 = 2$ μM), chosen with a reference to the concentration interval suitable for membrane permeabilization (Mally et al. 2007). The dependence of different features of the system (i.e., pore sizes, peptide-to-lipid ratio and membrane-permeability values) on the MLT concentration has been examined in numerous studies (Raghuraman and Chattopadhyay 2007), and by finding the MLT-induced membrane permeability in our previous work it was also shown to increase both with time and MLT concentration. In this study the work was focused on elucidating the mechanisms of pore formation to find the causes for the membrane-permeability increase. An implicit result of the study exemplifies that with an increased bulk concentration of MLT, the numbers of pores in the membrane are larger (as illustrated in Fig. 8).

Based on the findings of our previous work with MLT at low concentrations (Mally et al. 2007), MLT pairs serve as vehicles for lipid molecules to flow from the outer to the inner membrane leaflet, possibly by shortly stabilizing small lipid pores, whereas the probability for another MLT monomer to encounter a short-lived pore increases with MLT concentration. MLT pairs were therefore assumed to act as precursors to pores with three or more monomers, which is also a feature of the suggested model in the present work. In the study on the kinetics of the MLT pore formation, Schwarz et al. (1992) stressed dimerization to be a key step of the process; in a study on MLT-induced permeabilization Takei et al. (1999) also provided evidence for the kinetic importance of MLT dimerization in the pore formation process at higher concentrations of MLT.

The pore growth is thus supported by the electrostatic repulsion between the involved MLT monomers and by the energetically favorable joining of a MLT molecule into a pore rim (Mihajlovic and Lazaridis 2010). As described before, the fraction of MLT monomers (lying parallel in the membrane) diminishes rapidly as they become massively involved in pore rims and change their orientation by adopting their trans-bilayer positions (Fig. 6c). This result is in accord with the conclusion of the study by Huang et al. (2004) where the results of the experiments with MLT and GUVs (Longo et al. 1998) were interpreted, and it was suggested that pore formation resembles a phase transition from a state with no pores to a state of multiple pores. Their model predicted that the formed pores are of the same size, whereas our model yields the continuous reformation of pores with a narrowing pore size distribution in the membrane over time, peaking at a pore size with minimal energy. Despite the continuously changing pore distribution in the membrane, we can therefore deduce

relatively stable properties of an "average MLT pore". The average pore radius $<R_p>$ is reached (around 1.3 nm) during the time of a typical experiment (Fig. 8b), in agreement with numerous reports on the MLT pore diameter (Raghuraman and Chattopadhyay 2007). The pore size first increases and is then stabilized at a slightly lower value as the larger pores undergo fission; a similar observation was reported in a recent study by Fuertes et al. (2010), where the permeabilization of GUVs was induced by an amphipathic cationic peptide Baxα5 and the pores exhibited a relaxation toward a smaller size when approaching stationary conditions.

On the basis of the presented measurement data analysis, we can also discuss the possible reasons for a consistently observed, variable time lag, i.e., a concentration plateau referring to an unchanged level of solute concentration inside the vesicle in the time interval between the transfer of a giant vesicle into the solution with MLT and the beginning of the measurable solute leakage from the vesicle. The modeled pore formation process only accounts for a part of the time-lag interval (indicated by arrows in Fig. 3). We presumed that the beginning of the pore formation is a stochastic process and that a membrane defect is required to stabilize a short-lived dimer for long enough for an additional monomer to drift to the curved part of the MLT-dimer-induced membrane opening and in that way stabilize the pore rim: the model scenario assumes that MLT partitions from the bulk solution continuously and is present in the membrane in monomeric and dimeric forms. Only if a stochastic pore-nucleation event takes place (at time $t'$) is a process of pore formation triggered, enabling the pores (with $n \geq 3$) to grow and making the transport of solutes possible when the pores are large enough. The hypothesis of a stochastic pore formation has been considered in many studies (Sengupta et al. 2008; Tamba et al. 2010) and is supported by the fact that there was a significant fraction of vesicles that were not permeabilized during typical experimental times ($\approx$20 min) in this study (reported also by Lee et al. 2008). Similarly the studies of the antimicrobial peptides affecting individual bacteria report on stochastic onset of the peptides' action (Fantner et al. 2010). At this point we cannot give a satisfactory explanation for the considerable partition coefficient variability; however, related to this problem a correlation was noted among the time-lag interval, $k_{on,0}$ parameter (proportional to partition coefficient) and the age of the vesicles (the number of days since the preparation of the vesicles). The beginning of the permeabilization process seems to be triggered later, and the $k_{on,0}$ parameter has a lower value in the older vesicles membranes, suggesting that at least a part of the effect could be attributed to a change in the MLT-membrane interaction parameters as the membrane ages.

**Acknowledgments** This work was supported by the Slovenian Research Agency through grant P1-0055. The experiments comply with the laws of the Republic of Slovenia.

**Conflict of interest** The authors declare that they have no conflict of interest.

## References

Allende D, Simon SA, McIntosh TJ (2005) Melittin-induced bilayer leakage depends on lipid material properties: evidence for toroidal pores. Biophys J 88:1828–1837

Angelova MI, Soleau S, Meleard P, Faucon JF, Bothorel P (1992) Preparation of giant vesicles by external AC fields. Prog Colloid Polym Sci 89:127–131

Beschiaschvili G, Seelig J (1990) Melittin binding to mixed phosphatidylglycerol/phosphatidylcholine membranes. Biochemistry 29:52–58

Bohrer MP, Deen WM, Robertson CR, Troy JL, Brenner BM (1979) Influence of molecular configuration on the passage of macromolecules across the glomerular capillary wall. J Gen Physiol 74:583–593

Chen FY, Lee MT, Huang HW (2003) Evidence for membrane thinning effect as the mechanism for peptide-induced pore formation. Biophys J 84:3751–3758

Dempsey CE (1990) The actions of melittin on membranes. Biochim Biophys Acta 1031:143–161

dos Santos Cabrera MP, de Souza BM, Fontana R, Konno K, Palma MS, de Azevedo WF Jr, Ruggiero Neto J (2004) Conformation and lytic activity of eumenine mastoparan: a new antimicrobial peptide from wasp venom. J Peptide Res 64:95–103

Fantner GE, Barbero RJ, Belcher AM (2010) Kinetics of antimicrobial peptide activity measured on individual bacterial cells using high-speed atomic force microscopy. Nat Nanotechnol 5:280–285

Fuertes G, García-Sáez AJ, Esteban-Martín S, Giménez D, Sánchez-Muñoz OL, Schwille P, Salgado J (2010) Pores formed by Baxα5 relax to a smaller size and keep at equilibrium. Biophys J 99:2917–2925

Hamm EC, Simson DA, Merkel R, Smetacek V (1999) Colonies of *Phaeocystis globosa* are protected by a thin but tough skin. Mar Ecol Prog Ser 187:101–111

Heyman NS, Burt JM (2008) Hindered diffusion through an aqueous pore describes invariant dye selectivity of Cx43 junctions. Biophys J 94:840–854

Hristova K, Dempsey CE, White SH (2001) Structure, location and lipid perturbations of melittin at the membrane interface. Biophys J 80:801–811

Huang HW, Chen FY, Lee MT (2004) Molecular mechanism of peptide—induced pores in membranes. Phys Rev Lett 92:198304-1-4

Karatekin E, Sandre O, Guitouni H, Borghi N, Puech PH, Brochard-Wyart F (2003) Cascades of transient pores in giant vesicles: line tension and transport. Biophys J 84:1734–1749

Katsu T, Ninomiya C, Kuroko M, Kobayashi H, Hirota T, Fujita Y (1988) Action mechanism of amphipathic peptides on erythrocyte membrane. Biochim Biophys Acta 939:57–63

Kuchinka E, Seelig J (1989) Interaction of melittin with phosphatidylcholine membranes. Binding isotherm and lipid head-group conformation. Biochemistry 28:4216–4221

Ladokhin AS, Selsted ME, White SH (1997) Sizing membrane pores in lipid vesicles by leakage of co-encapsulated markers: pore formation by melittin. Biophys J 72:1762–1766

Lee MT, Chen FY, Huang HW (2004) Energetics of pore formation induced by membrane active peptides. Biochemistry 43:3590–3599

Lee MT, Hung WC, Chen FY, Huang HW (2008) Mechanism and kinetics of pore formation in membranes by water-soluble amphipathic peptides. Proc Natl Acad Sci USA 105:5087–5092

Lin JH, Baumgaertner A (2000) Stability of a melittin pore in a lipid bilayer: a molecular dynamics study. Biophys J 78:1714–1724

Longo ML, Waring AJ, Gordon LM, Hammer DA (1998) Area expansion and permeation of phospholipid membrane bilayer by influenza fusion peptides and melittin. Langmuir 14:2385–2395

Macháň R, Miszta A, Hermens W, Hof M (2010) Real-time monitoring of melittin-induced pore and tubule formation from supported lipid bilayers and its physiological relevance. Chem Phys Lipids 163:200–206

Mally M, Majhenc J, Svetina S, Žekš B (2002) Mechanisms of equinatoxin II—induced transport through the membrane of a giant phospholipids vesicle. Biophys J 83:944–953

Mally M, Majhenc J, Svetina S, Žekš B (2007) The response of giant phospholipid vesicles to pore-forming peptide melittin. Biochim Biophys Acta 1768:1179–1189

Manna M, Mukhopadhyay C (2009) Cause and effect of melittin-induced pore formation: a computational approach. Langmuir 25:12235–12242

Matsuzaki K, Yoneyama S, Miyajima K (1997) Pore formation and translocation of melittin. Biophys J 73:831–838

Mihajlovic M, Lazaridis T (2010) Antimicrobial peptides bind more strongly to membrane pores. Biochim Biophys Acta 1798:1494–1502

Naito A, Nagao T, Norisada K, Mizuno T, Tuzi S, Saitô H (2000) Conformation and dynamics of melittin bound to magnetically oriented lipid bilayers by solid-state $^{31}P$ and $^{13}C$ NMR spectroscopy. Biophys J 78:2405–2417

Pluta M (1989) Advanced light microscopy, vol 2. Elsevier, Amsterdam

Raghuraman H, Chattopadhyay A (2007) Melittin: a membrane-active peptide with diverse functions. Biosci Rep 27:189–223

Rasband WS (1997–2012) ImageJ. US NIH, Bethesda. http://imagej.nih.gov/ij/

Rex S, Schwarz G (1998) Quantitative studies on the melittin-induced leakage mechanism of lipid vesicles. Biochemistry 37:2336–2345

Schwarz G (1996) Electrical interactions of membrane active peptides at lipid/waterinterfaces. Biophys Chem 58:67–73

Schwarz G, Zong RT, Popescu T (1992) Kinetics of melittin induced pore formation in the membrane of lipid vesicles. Biochim Biophys Acta 1110:97–104

Sengupta D, Leontiadou H, Mark AE, Marrink SJ (2008) Toroidal pores formed by antimicrobial peptides show significant disorder. Biochim Biophys Acta 1778:2308–2310

Takei J, Remenyi A, Dempsey CE (1999) Generalised bilayer perturbation from peptide helix dimerisation at membrane surfaces: vesicle lysis induced by disulphide-dimerised melittin analogues. FEBS Lett 442:11–14

Tamba Y, Ariyama H, Levadny V, Yamazaki M (2010) Kinetic pathway of antimicrobial peptide magainin 2-induced pore formation in lipid membranes. J Phys Chem B 114:12018–12026

Terwilliger TC, Eisenberg D (1982) The structure of melittin. J Biol Chem 257:6016–6022

Torrens F, Castellano G, Campos A, Abad C (2007) Negatively cooperative binding of melittin to neutral phospholipid vesicles. J Mol Struct 834:216–228

Venturoli D, Rippe B (2005) Ficoll and dextran vs. globular proteins as probes for testing glomerular permselectivity: effects of molecular size, shape, charge, and deformability. Am J Physiol Renal Physiol 288:605–613

Yang L, Harroun TA, Weiss TM, Ding L, Huang HW (2001) Barrel-stave model or toroidal model? A case study on melittin pores. Biophys J 81:1475–1485

Zemel A, Fattal DR, Ben-Shaul A (2003) Energetics and self-assembly of amphipathic peptide pores in lipid membranes. Biophys J 84:2242–2255